Journal of Computational Mathematics
Vol.31, No.6, 2013, 573–591.

http://www.global-sci.org/jcm
doi:10.4208/jcm.1309-m3592

ON THE QUASI-RANDOM CHOICE METHOD FOR THE LIOUVILLE EQUATION OF GEOMETRICAL OPTICS WITH DISCONTINUOUS WAVE SPEED*

Jingwei Hu
Institute for Computational Engineering and Sciences (ICES), The University of Texas at Austin, 201 East 24th St, Stop C0200, Austin, TX 78712, USA
Email: hu@ices.utexas.edu
Shi Jin
Department of Mathematics, University of Wisconsin-Madison, 480 Lincoln Drive, Madison, WI 53706, USA
Department of Mathematics, Institute of Natural Sciences, and MOE Key Lab in Scientific and Engineering Computing, Shanghai Jiao Tong University, Shanghai 200240, China
Email: jin@math.wisc.edu

Abstract

We study the quasi-random choice method (QRCM) for the Liouville equation of geometrical optics with *discontinuous* local wave speed. This equation arises in the phase space computation of high frequency waves through interfaces, where waves undergo partial transmissions and reflections. The numerical challenges include interface, contact discontinuities, and measure-valued solutions. The so-called QRCM is a random choice method based on quasi-random sampling (a deterministic alternative to random sampling). The method not only is viscosity-free but also provides faster convergence rate. Therefore, it is appealing for the problem under study which is indeed a Hamiltonian flow. Our analysis and computational results show that the QRCM 1) is almost first-order accurate even with the aforementioned discontinuities; 2) gives sharp resolutions for all discontinuities encountered in the problem; and 3) for measure-valued solutions, does not need the level set decomposition for finite difference/volume methods with numerical viscosities.

Mathematics subject classification: 35L45, 65M06, 11K45.
Key words: Liouville equation, High frequency wave, Interface, Measure-valued solution, Random choice method, Quasi-random sequence.

1. Introduction

In this paper, we study a type of Monte Carlo methods for numerical computation of the Liouville equation in geometrical optics. Let $f(\mathbf{x}, \mathbf{v}, t)$ be the energy density distribution of waves that depends on position $\mathbf{x}$, slowness vector $\mathbf{v}$, and time t, then the Liouville equation reads

$$f_t + \nabla_{\mathbf{v}} H \cdot \nabla_{\mathbf{x}} f - \nabla_{\mathbf{x}} H \cdot \nabla_{\mathbf{v}} f = 0, \quad t > 0, \ \mathbf{x}, \mathbf{v} \in \mathbb{R}^d, \tag{1.1}$$

where the Hamiltonian H is given by

$$H(\mathbf{x}, \mathbf{v}) = c(\mathbf{x})|\mathbf{v}| \tag{1.2}$$

* Received December 23, 2010 / Revised version received July 28, 2013 / Accepted September 16, 2013 / Published online October 18, 2013 /

with $c(\mathbf{x})$ being the local wave speed of the medium. The bicharacteristics of equation (1.1) satisfy the Hamiltonian system:

$$\frac{d\mathbf{x}}{dt} = c\frac{\mathbf{v}}{|\mathbf{v}|}, \quad \frac{d\mathbf{v}}{dt} = -\nabla_{\mathbf{x}} c|\mathbf{v}|. \tag{1.3}$$

The Liouville equation (1.1) arises in the phase space description of geometrical optics. It can be derived as the high frequency limit of the wave equation

$$u_{tt} - c(\mathbf{x})^2 \Delta u = 0 \tag{1.4}$$

via the Wigner transform [1–3]. It is also the basis of computing multi-valued physical observables [4–8].

We are particularly interested in the case when $c(\mathbf{x})$ contains discontinuities due to different refractive indices at different media. The discontinuity corresponds to an interface, at which incoming waves can be partially transmitted and reflected. Against this background, much work has been done in the past both analytically [9–12] and numerically [13–18]. Numerically this problem consists of three challenges:

(1) One needs to provide an interface condition at the discontinuities of $c(\mathbf{x})$ to account for partial transmissions and reflections. This was first done in [13, 14], where the interface conditions (consistent to Snell's law) were built into numerical fluxes — the so-called Hamiltonian-preserving (HP) scheme.

(2) Due to the transmissions and reflections, f becomes discontinuous which then propagates linearly along the bicharacteristics (1.3). These are linear (contact) discontinuities that will be smeared by a typical finite difference or finite volume method, which necessarily contains numerical viscosities to suppress numerical oscillations across the discontinuities, with the smearing zone increases with time [19].

(3) The Liouville equation arising in geometrical optics or semiclassical limit involves measure-valued initial condition of delta-function shape:

$$f(\mathbf{x}, \mathbf{v}, 0) = \rho_0(\mathbf{x})\delta(\mathbf{v} - \mathbf{u}_0(\mathbf{x})). \tag{1.5}$$

The solution at later time remains measure-valued (with finite or even infinite number of concentrations corresponding to caustics in the physical space). For this type of problem, finite difference/volume methods usually produce poor quality results as the approximate delta functions are quickly smeared out due to numerical dissipation. The level set method proposed in [20] decomposes f into ϕ and ψ_i $(i = 1, \ldots, d)$, where ϕ and ψ_i solve the same Liouville equation with initial data

$$\phi(\mathbf{x}, \mathbf{v}, 0) = \rho_0(\mathbf{x}), \quad \psi_i(\mathbf{x}, \mathbf{v}, 0) = v_i - u_{0i}(\mathbf{x}) \tag{1.6}$$

respectively. The density and averaged slowness can then be recovered by taking the moments of f:

$$\rho(\mathbf{x}, t) = \int_{\mathbb{R}^d} f(\mathbf{x}, \mathbf{v}, t)\, d\mathbf{v} = \int_{\mathbb{R}^d} \phi \,\Pi_{i=1}^d \delta(\psi_i)\, d\mathbf{v}, \tag{1.7}$$

$$\mathbf{u}(\mathbf{x}, t) = \frac{1}{\rho(\mathbf{x}, t)} \int_{\mathbb{R}^d} f(\mathbf{x}, \mathbf{v}, t)\mathbf{v}\, d\mathbf{v} = \frac{1}{\rho(\mathbf{x}, t)} \int_{\mathbb{R}^d} \phi \,\Pi_{i=1}^d \delta(\psi_i)\mathbf{v}\, d\mathbf{v}. \tag{1.8}$$

This approach allows the computation of bounded rather than measure-valued solutions, which greatly enhances the numerical resolution. However, as pointed out in [8, 14], it only readily

works for *complete* transmissions and reflections. For the case of *partial* transmissions and reflections, a new level set function has to be added every time the wave hits the interface in order to track all reflection and refraction branches, thus making the method unfeasible for multiple interfaces and long computation time. The recent work by Wei et al [18] suggested a way to handle this problem by the level set method, but it needs an initialization procedure at every time step.

The random choice method (RCM), or the Glimm's scheme, was first introduced by Glimm in 1965 for proving the existence of global weak solutions to hyperbolic system of conservation laws [21]. Later it was used as a numerical tool by Chorin in gas dynamics [22,23]. Chorin's work was followed by numerous researchers, with applications and further improvements in [24–26], and more recently [27, 28], etc. The main advantage of this method is the sharp resolutions of shocks and especially, contact discontinuities. In addition, as first investigated by Colella [26], if the quasi-random sequence rather than random or pseudo-random sequence is used in RCM for sampling, one can improve the convergence rate from $O(1/\sqrt{N})$ to $O(\log N/N)$[1)] . The resulting RCM which we will call the quasi-random choice method (QRCM) in the sequel, due its lack of numerical viscosity, seems to be a natural choice to overcome some of the aforementioned difficulties, since the original Liouville equation is indeed a Hamiltonian (non-dissipative) system characterized by (1.2).

We would like to mention that the QRCM is restricted to first-order accuracy. The value of this study is to demonstrate its sharp resolutions for both contact discontinuities and measure-valued solutions that are typical in high frequency waves through interfaces. Away from singular regions, higher order methods are more desirable, so it seems to us that a hybrid method that combines the QRCM with a higher order scheme will offer the best numerical results. Such a hybrid method is not very difficult to construct as the Liouville equation is linear [29].

The rest of the paper is organized as follows. In the next section, we introduce the original RCM and extend it to the 2-D linear advection equation that are relevant to solving multi-D phase space equations. In Section 3, we describe the QRCM and its basic properties (a rigorous L^1-error estimate is given in the appendix for the linear equation with bounded variation (BV) initial data). In Section 4, a QRCM combined with HP scheme is constructed for the Liouville equation with discontinuous wave speed. Numerical examples in both 1-D and 2-D are presented in Section 5 to illustrate the performance of QRCM for discontinuous and measure-valued solutions.

2. The Random Choice Method

We first describe the original RCM for the 1-D hyperbolic conservation law. There are two versions of the method in the literature: one uses a staggered grid; the other uses a single grid. We present the latter here for simplicity.

Consider the initial value problem:

$$u_t + q(u)_x = 0, \quad t > 0,\ x \in \mathbb{R}, \tag{2.1}$$

$$u(x, 0) = u_0(x), \quad x \in \mathbb{R}. \tag{2.2}$$

Divide the spatial domain into a number of cells $\left[x_{i-\frac{1}{2}}, x_{i+\frac{1}{2}}\right)$ with $x_{i+\frac{1}{2}} = \left(i + \frac{1}{2}\right) h$, $i \in \mathbb{Z}$. Each cell is centered at $x_i = ih$ of length h. Assume k is the time step size, and define $t_n = nk$,

[1)] This resembles $O(1/\sqrt{N})$ and $O(\log N/N)$ convergence rates of Monte-Carlo and quasi-Monte Carlo methods for numerical integration in 1-D.

$n = 0, 1, 2, \ldots$. Let $\mathbf{U}^n$ be the approximate solution at time t_n which is piecewise constant with value U_i^n on the cell $\left[x_{i-\frac{1}{2}}, x_{i+\frac{1}{2}}\right)$. The solution $\mathbf{U}^{n+1}$ at t_{n+1} is constructed as follows:

Step 1. *Solve equation (2.1) accurately with initial data* $\mathbf{U}^n$. *This is equivalent to solve a Riemann problem on each interval* $[ih, (i+1)h)$. *We impose the CFL condition*

$$\|q'\|_{L^\infty(\mathbb{R})} \frac{k}{h} \le \frac{1}{2}, \tag{2.3}$$

such that waves from adjacent intervals won't interact with each other by time t_{n+1}. *Define the exact solution* $\mathbf{U}_e$ *by piecing together all Riemann problem solutions.*

Step 2. *Choose a random number* ξ^{n+1} *uniformly distributed on interval* $[0, 1]$ *and take*

$$U_i^{n+1} = \mathbf{U}_e\left(\left(i - \frac{1}{2} + \xi^{n+1}\right) h, (n+1)k\right), \tag{2.4}$$

thus one obtains the approximate solution $\mathbf{U}^{n+1}$.

If the Eq. (2.1) is linear, i.e., $q(u) = au$, where a is a constant, the above scheme can be simplified as

$$\text{for } a > 0, \quad U_i^{n+1} = \begin{cases} U_{i-1}^n & \text{with probability } \dfrac{ak}{h}, \\ U_i^n & \text{with probability } 1 - \dfrac{ak}{h}; \end{cases} \tag{2.5}$$

$$\text{for } a < 0, \quad U_i^{n+1} = \begin{cases} U_{i+1}^n & \text{with probability } -\dfrac{ak}{h}, \\ U_i^n & \text{with probability } 1 + \dfrac{ak}{h}. \end{cases} \tag{2.6}$$

So in each time step, all function values will either stay there or move a distance h to the right or left (note that one random number is generated per time step and used for all cells). Therefore, the RCM has no numerical diffusion and the discontinuity remains perfectly sharp. Besides, the CFL condition (2.3) can be relaxed to

$$|a| \frac{k}{h} \le 1, \tag{2.7}$$

for all the waves travel with the same speed a (they won't interact at all). Recall that a first-order upwind scheme for the same equation reads:

$$\text{for } a > 0, \quad U_i^{n+1} = \frac{ak}{h} U_{i-1}^n + \left(1 - \frac{ak}{h}\right) U_i^n; \tag{2.8}$$

$$\text{for } a < 0, \quad U_i^{n+1} = -\frac{ak}{h} U_{i+1}^n + \left(1 + \frac{ak}{h}\right) U_i^n. \tag{2.9}$$

Hence, unlike the RCM treats U_i^{n+1} as a random variable, the finite difference scheme takes some kind of average — the expected value.

Since the Liouville equation is a linear equation in phase space, what is more relevant in our context is the following 2-D advection equation

$$u_t + au_x + bu_y = 0, \quad t > 0,\ x, y \in \mathbb{R}, \tag{2.10}$$

$$u(x, y, 0) = u_0(x, y), \quad x, y \in \mathbb{R}. \tag{2.11}$$

Let us first write down the upwind scheme for (2.10):

$$U_{i,j}^{n+1} = \left(1 - \frac{|a|k}{h} - \frac{|b|k}{h}\right) U_{i,j}^n + \frac{|a|k}{h} U_{i-\mathrm{sgn}(a),j}^n + \frac{|b|k}{h} U_{i,j-\mathrm{sgn}(b)}^n, \tag{2.12}$$

where the same discretization is used for both x and y. Analogously to the 1-D case, we can construct the RCM as follows:

$$U_i^{n+1} = \begin{cases} U_{i-\mathrm{sgn}(a),j}^n & \text{with probability } \dfrac{|a|k}{h}, \\ U_{i,j-\mathrm{sgn}(b)}^n & \text{with probability } \dfrac{|b|k}{h}, \\ U_{i,j}^n & \text{with probability } 1 - \dfrac{|a|k}{h} - \dfrac{|b|k}{h}, \end{cases} \tag{2.13}$$

and the CFL condition becomes

$$|a|\frac{k}{h} + |b|\frac{k}{h} \le 1. \tag{2.14}$$

To analyze the numerical error in scheme (2.13), let U_{i_0,j_0}^0 be the initial value of the solution at (x_{i_0}, y_{j_0}), and η_k be the displacement of U_{i_0,j_0}^0 at each time step. Clearly η_k's are the i.i.d. random variables that satisfy

$$\begin{cases} \mathbb{P}(\eta_k = (\mathrm{sgn}(a)h, 0)) = \dfrac{|a|k}{h}, \\ \mathbb{P}(\eta_k = (0, \mathrm{sgn}(b)h)) = \dfrac{|b|k}{h}, \\ \mathbb{P}(\eta_k = (0,0)) = 1 - \dfrac{|a|k}{h} - \dfrac{|b|k}{h}, \end{cases} \tag{2.15}$$

where $\mathbb{P}$ represents the probability. The expected value and the variance of η_k are then given by

$$\mathbb{E}[\eta_k] = (ak, bk), \quad \mathrm{Var}[\eta_k] = (|a|kh - a^2k^2, |b|kh - b^2k^2). \tag{2.16}$$

Suppose after n time steps U_{i_0,j_0}^0 is at $(x_{i_0}, y_{j_0}) + \eta$, where $\eta = \sum_{k=1}^n \eta_k$ is the total displacement. We have

$$\mathbb{E}[\eta] = \sum_{k=1}^n \mathbb{E}[\eta_k] = (at_n, bt_n), \tag{2.17}$$

$$\mathrm{Var}[\eta] = \sum_{k=1}^n \mathrm{Var}[\eta_k] = \left(|a|ht_n\left(1 - \frac{|a|k}{h}\right), |b|ht_n\left(1 - \frac{|b|k}{h}\right)\right). \tag{2.18}$$

Thus the expected value of η is just the exact displacement. The variance implies that the location error is of order $\sqrt{ht_n}$ (assume k/h is constant). Indeed, Lucier [30] showed that the expected error of RCM in $L^1(\mathbb{R})$ at time t_n for the 1-D conservation law (2.1) (2.2) is bounded by

$$\left(h + \frac{2}{\sqrt{3}}\sqrt{\frac{h}{k}}\sqrt{ht_n}\right)\|u_0\|_{BV(\mathbb{R})}, \tag{2.19}$$

where $\|u_0\|_{BV(\mathbb{R})}$ is the total variation of u_0 on $\mathbb{R}$.

3. The Quasi-Random Choice Method

In [26], Colella suggested using the *quasi-random* sequences instead of *random* or *pseudo-random* sequences in the RCM. The quasi-random (also called low-discrepancy) sequence is purely deterministic: the points in it are correlated to provide greater uniformity [31]. As a consequence, the resulting RCM (QRCM) can be shown to have a faster convergence rate. Compared to (2.19), the spatial error is improved from $O(\sqrt{h})$ to $O(|\log h|\, h)$; the temporal growth factor is reduced from $O(\sqrt{t_n})$ to $O(\log t_n)$ (see the appendix for a rigorous proof).

The general idea can be illustrated by a simple example. The argument follows that in [26]. Still consider the 2-D equation (2.10), and as previously let $U^0_{i_0,j_0}$ be the initial value of the solution at grid point (x_{i_0}, y_{j_0}). We define the location of this value at time t_n by

$$
\begin{aligned}
&l_0 = (x_{i_0}, y_{j_0}),\\
&l_n = \begin{cases}
l_{n-1} + \operatorname{sgn}(a)(h,0), & \text{if } \xi^n \in \left[0, \dfrac{|a|k}{h}\right) = I_1,\\
l_{n-1} + \operatorname{sgn}(b)(0,h), & \text{if } \xi^n \in \left[\dfrac{|a|k}{h}, \dfrac{|a|k}{h} + \dfrac{|b|k}{h}\right) = I_2,\\
l_{n-1}, & \text{otherwise,}
\end{cases}
\end{aligned}
\tag{3.1}
$$

where $\boldsymbol{\xi} = \xi^1, \xi^2, \ldots, \xi^n, \ldots$ is taken as a quasi-random sequence.

A sequence $\boldsymbol{\xi}$ is said to be *equidistributed* if for any subinterval I in $[0,1]$, the proportion of times that ξ^j lies in I is asymptotically equal to $|I|$, the length of I; i.e., if one defines

$$
\frac{N\{j = 1, \ldots, n;\ \xi^j \in I\}}{n} - |I| = \delta(\boldsymbol{\xi}, n, I),
\tag{3.2}
$$

then $\boldsymbol{\xi}$ is equidistributed if

$$
D_n = \sup_{I \subset [0,1]} |\delta(\boldsymbol{\xi}, n, I)| \to 0, \quad \text{as } n \to \infty,
\tag{3.3}
$$

where D_n is called the *discrepancy* of the sequence. $\boldsymbol{\xi}$ is said to be *quasi-random* if

$$
D_n \le C \frac{\log n}{n},
\tag{3.4}
$$

in which C is a constant independent of n.

With the above definition, we can express l_n in (3.1) as

$$
\begin{aligned}
l_n &= l_0 + N\left\{j = 1, 2, \ldots, n;\ \xi^j \in I_1\right\} \cdot \operatorname{sgn}(a)(h,0)\\
&\quad + N\left\{j = 1, 2, \ldots, n;\ \xi^j \in I_2\right\} \cdot \operatorname{sgn}(b)(0,h)\\
&= l_0 + \left(\frac{ak}{h} + \operatorname{sgn}(a)\delta(\boldsymbol{\xi}, n, I_1)\right)(nh, 0) + \left(\frac{bk}{h} + \operatorname{sgn}(b)\delta(\boldsymbol{\xi}, n, I_2)\right)(0, nh)\\
&= l_0 + (at_n, bt_n) + \frac{h}{k} t_n (\operatorname{sgn}(a)\delta(\boldsymbol{\xi}, n, I_1), \operatorname{sgn}(b)\delta(\boldsymbol{\xi}, n, I_2)).
\end{aligned}
\tag{3.5}
$$

Therefore, the error between l_n and the exact location $l_0 + (at_n, bt_n)$ is bounded by

$$
C_1 \frac{h}{k} t_n \frac{\log n}{n},
\tag{3.6}
$$

which goes to zero as $n \to \infty$, when t_n and h/k fixed. Furthermore, since $n = O(1/h)$, this error is of order $O(|\log h|\, h)$, better than $O(\sqrt{h})$ of the random sequence based RCM.

The simplest example of a quasi-random sequence is the van der Corput sequence [32]. It is constructed by reversing the base b representation of the sequence of natural numbers. In the binary case ($b = 2$), let

$$n = \sum_{k=0}^{m} i_k 2^k, \quad i_k = 0, 1 \tag{3.7}$$

be the binary expansion of $n = 1, 2, \ldots$, then

$$\xi^n = \sum_{k=0}^{m} i_k 2^{-(k+1)}. \tag{3.8}$$

We will use this sequence in our numerical simulation.

Remark 3.1. The quasi-random sequences applied to Monte-Carlo integration is a popular research topic in mathematical finance. The in-depth study of their properties is beyond the scope of the paper. A nice review can be found in [33].

4. A Quasi-Random Choice Scheme for the Liouville Equation with Discontinuous Wave Speed

In this section, we present the numerical scheme for the Liouville equation (1.1), which is a combination of the QRCM and the HP scheme [14]. For discontinuous wave speed $c(\mathbf{x})$, the combined method not only captures the correct physics (attributed to HP scheme) but also provides sharp resolutions at contact discontinuities induced by the interface (attributed to QRCM). For generality, the scheme will be given for the 2-D case (2-D for both spatial and slowness domain). Simplification to 1-D and extension to 3-D are straightforward.

Consider the 2-D Liouville equation:

$$f_t + \frac{c(x,y)u}{\sqrt{u^2+v^2}} f_x + \frac{c(x,y)v}{\sqrt{u^2+v^2}} f_y - c_x\sqrt{u^2+v^2} f_u - c_y\sqrt{u^2+v^2} f_v = 0. \tag{4.1}$$

Assume a uniform mesh for all directions x, y, u, v: the phase space is divided into a number of cells with boundaries at $x_{i+\frac{1}{2}}$, $y_{j+\frac{1}{2}}$, $u_{k+\frac{1}{2}}$, $v_{l+\frac{1}{2}}$, and the cells are centered at (x_i, y_j, u_k, v_l) with sidelength h. The time domain is discretized as before: $t_n = nk$ with step size k. We approximate $c(x, y)$ by a piecewise bilinear function, and always provide two interface values at each cell interface, e.g., $c^-_{i+\frac{1}{2},j}$ and $c^+_{i+\frac{1}{2},j}$ at $x_{i+\frac{1}{2},j}$, when c is smooth at $x_{i+\frac{1}{2},j}$, the two values are identical. Therefore, the derivatives c_x and c_y in the cell (i, j, k, l) can be approximated by

$$c_x \approx \frac{c^-_{i+\frac{1}{2},j} - c^+_{i-\frac{1}{2},j}}{h}, \quad c_y \approx \frac{c^-_{i,j+\frac{1}{2}} - c^+_{i,j-\frac{1}{2}}}{h}. \tag{4.2}$$

Since the interfaces lie in the spatial domain, the main difficulty of solving (4.1) comes from the transport terms in the (x, y) plane. To simplify the problem, in what follows, we will assume the wave speed c as a piecewise constant function, so the equation (4.1) becomes

$$f_t + \frac{c(x,y)u}{\sqrt{u^2+v^2}} f_x + \frac{c(x,y)v}{\sqrt{u^2+v^2}} f_y = 0. \tag{4.3}$$

The combined QRCM and HP scheme for (4.3) when $\frac{c(x,y)u}{\sqrt{u^2+v^2}} > 0$ and $\frac{c(x,y)v}{\sqrt{u^2+v^2}} < 0$ is given in Algorithm 4.1 (other cases are treated similarly).

Algorithm 4.1 The combined QRCM and HP scheme for the 2-D Liouville equation (4.3).

for each t_{n+1} **do**
  fetch a new quasi-random number ξ^{n+1} from the van der Corput sequence;
  for each x_i, y_j, u_k, v_l **do**
    $a_{i,j} = c_{i,j}\frac{u_k}{\sqrt{u_k^2+v_l^2}}$; $b_{i,j} = c_{i,j}\frac{v_l}{\sqrt{u_k^2+v_l^2}}$;
    if $\xi^{n+1} < \frac{a_{i,j}k}{h}$ **then**
      if at the cell (i,j,k,l) right to the interface $(x_{i-\frac{1}{2}}, y_j)$ **then**
        $u_R = -u_k$;
        if $w = \left(\frac{c^+_{i-\frac{1}{2},j}}{c^-_{i-\frac{1}{2},j}}\right)^2 u_k^2 + \left[\left(\frac{c^+_{i-\frac{1}{2},j}}{c^-_{i-\frac{1}{2},j}}\right)^2 - 1\right] v_l^2 > 0$ **then**
          $u_T = \sqrt{w}$; find index m such that $u_{m-1} < u_T < u_m$;
          $\gamma^{in} = \frac{u_T}{\sqrt{u_T^2+v_l^2}}$; $\gamma^{tr} = \frac{u_k}{\sqrt{u_k^2+v_l^2}}$; $\alpha^R = \left(\frac{c^+_{i-\frac{1}{2},j}\gamma^{in} - c^-_{i-\frac{1}{2},j}\gamma^{tr}}{c^+_{i-\frac{1}{2},j}\gamma^{in} + c^-_{i-\frac{1}{2},j}\gamma^{tr}}\right)^2$; $\alpha^T = 1-\alpha^R$;
          $f^{n+1}_{i,j,k,l} = \alpha^T\left(\frac{u_m-u_T}{h} f^n_{i-1,j,m-1,l} + \frac{u^T-u_{m-1}}{h} f^n_{i-1,j,m,l}\right) + \alpha^R f^n_{i,j,R,l}$;
        else
          $f^{n+1}_{i,j,k,l} = f^n_{i,j,R,l}$;
        end if
      else
        $f^{n+1}_{i,j,k,l} = f^n_{i-1,j,k,l}$;
      end if
    else if $\frac{a_{i,j}k}{h} < \xi^{n+1} < \frac{a_{i,j}k}{h} - \frac{b_{i,j}k}{h}$ **then**
      if at the cell (i,j,k,l) down to the interface $(x_i, y_{j+\frac{1}{2}})$ **then**
        $v_R = -v_l$;
        if $w = \left[\left(\frac{c^-_{i,j+\frac{1}{2}}}{c^+_{i,j+\frac{1}{2}}}\right)^2 - 1\right] u_k^2 + \left(\frac{c^-_{i,j+\frac{1}{2}}}{c^+_{i,j+\frac{1}{2}}}\right)^2 v_l^2 > 0$ **then**
          $v_T = -\sqrt{w}$; find index m such that $v_{m-1} < v_T < v_m$;
          $\gamma^{in} = \frac{-v_T}{\sqrt{u_k^2+v_T^2}}$; $\gamma^{tr} = \frac{-v_l}{\sqrt{u_k^2+v_l^2}}$; $\alpha^R = \left(\frac{c^-_{i,j+\frac{1}{2}}\gamma^{in} - c^+_{i,j+\frac{1}{2}}\gamma^{tr}}{c^-_{i,j+\frac{1}{2}}\gamma^{in} - c^+_{i,j+\frac{1}{2}}\gamma^{tr}}\right)^2$; $\alpha^T = 1-\alpha^R$;
          $f^{n+1}_{i,j,k,l} = \alpha^T\left(\frac{v_m-v_T}{h} f^n_{i,j+1,k,m-1} + \frac{v^T-v_{m-1}}{h} f^n_{i,j+1,k,m}\right) + \alpha^R f^n_{i,j,k,R}$;
        else
          $f^{n+1}_{i,j,k,l} = f^n_{i,j,k,R}$;
        end if
      else
        $f^{n+1}_{i,j,k,l} = f^n_{i,j+1,k,l}$;
      end if
    else
      $f^{n+1}_{i,j,k,l} = f^n_{i,j,k,l}$;
    end if
  end for
end for

5. Numerical Examples

In this section, we study the numerical performance of the algorithm in section 4 for the Liouville equation with discontinuous wave speed. The emphasis is given to measure-valued

solutions with partial transmissions and reflections at the interface. As mentioned in the introduction, the level set decomposing approach [20] does not work in this case, so a finite difference/volume method that directly evolves the approximate delta function is expected to have poor resolutions. We will show, however, the QRCM performs equally well for both bounded and measure-valued solutions, hence no special treatment of the delta function is needed.

Three different methods will be compared in the following: the first-order upwind scheme (referred to as *upwind*), the second-order Lax-Wendroff scheme with the van Leer flux limiter (referred to as *LW-lim*) [34], and the QRCM based on base 2 van der Corput sequence.

Example 4.1. We first consider the simple 1-D Liouville equation

$$f_t + c(x)\text{sign}(v)f_x - c_x|v|f_v = 0, \tag{5.1}$$

with bounded-value initial condition

$$f(x,v,0) = \begin{cases} 1, & x<0,\ v>0,\ \sqrt{x^2+4v^2}<1, \\ 1, & x>0,\ v<0,\ \sqrt{x^2+v^2}<1, \\ 0, & \text{otherwise.} \end{cases} \tag{5.2}$$

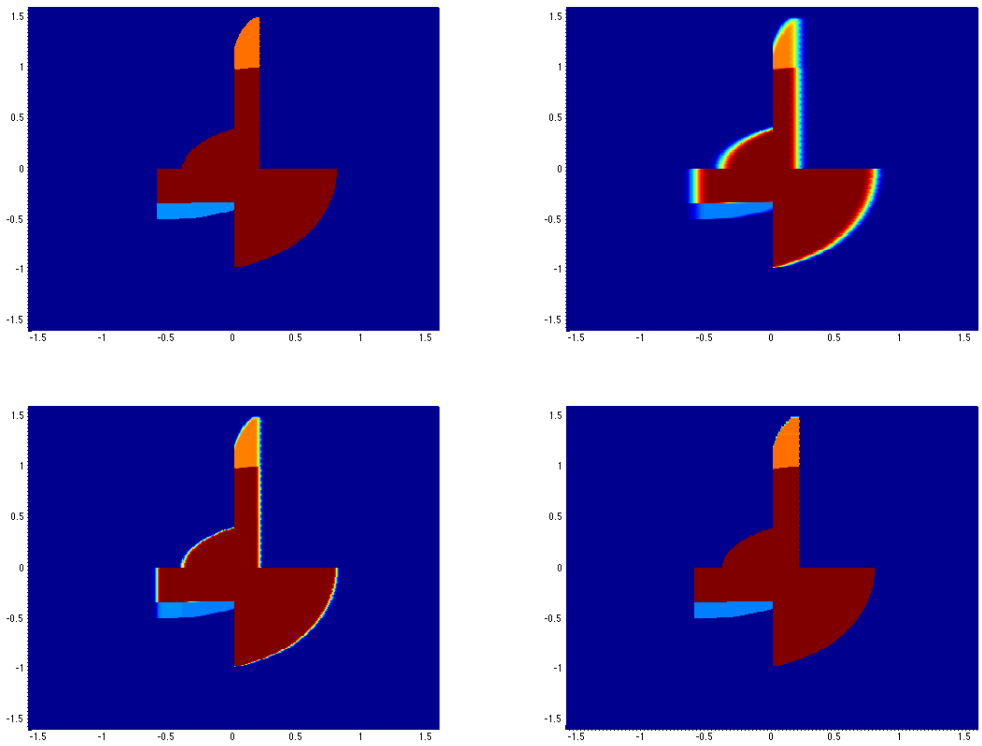

Fig. 5.1. Contour plots of the exact and numerical f at $t = 1$ on a 400×400 mesh. The horizontal axis is x, the vertical axis is v. $h = 0.008$. CFL condition: $k = h$. Upper left: exact solution; upper right: *upwind*; bottom left: *LW-lim*; bottom right: QRCM.

The wave speed $c(x)$ is assumed to be piecewise constant

$$c(x) = \begin{cases} 0.6, & x < 0, \\ 0.2, & x > 0. \end{cases} \tag{5.3}$$

So at the interface $x = 0$, the reflection and transmission coefficients are $\alpha^R = \frac{1}{4}$, $\alpha^T = \frac{3}{4}$.

The computational domain is chosen as $[x, v] \in [-1.6, 1.6] \times [-1.6, 1.6]$. The exact solution can be constructed by the method of characteristics, see [14] for its analytical form. Fig. 5.1 shows the contour plots of the exact and numerical solutions f at time $t = 1$. The upwind scheme smears the discontinuities severely. The resolution is improved in *LW-lim*, but there are still numerical viscosities. The random choice solution, although containing mild oscillations due to its random nature, has very sharp boundaries. We are also interested in macroscopic quantities such as density $\rho(x,t) = \int f(x,v,t)\,dv$ and averaged slowness $u(x,t) = \int f(x,v,t)v\,dv/\rho(x,t)$. The numerical solutions are given in Fig. 5.2.

In Table 5.1, we compare the l^1-errors of the three methods on different meshes. The convergence rate of the upwind scheme is about 0.5, which agrees with the well-established theory that the L^1-error of discontinuous solutions to the linear hyperbolic equation by monotone difference schemes is at most halfth order [35, 36]. For the QRCM, every time we compute a solution, a portion of the van der Corput sequence is used. The length of the selected sequence depends on the total time steps, and it is not necessary to always start from the beginning. As a result, the numerical solutions can be different for various starting indices[2)] . Here the numerical error is the average over 20 evaluations. One can see that the error of QRCM on a 160×160 mesh is already comparable to finite difference solutions on the fine 400×400 mesh.

Table 5.1: l^1-errors of f at $t = 1$, $k = h$.

meshes	80×80	160×160	240×240	320×320	400×400	convergence rate
upwind	0.2150	0.1577	0.1276	0.1108	0.0994	**0.48**
LW-lim	0.1168	0.0730	0.0535	0.0434	0.0370	**0.72**
QRCM (avg)	0.0727	0.0371	0.0221	0.0187	0.0135	**1.03**

Example 4.2. We next consider the 1-D Liouville equation (5.1) with mesure-valued initial condition

$$f(x, v, 0) = \delta(v - u_0(x)), \tag{5.4}$$

where

$$u_0(x) = \begin{cases} 0.5, & x \le -1.6, \\ 0.5 - \dfrac{0.4}{(1.6)^2}(x + 1.6)^2, & -1.6 < x \le 0, \\ -0.5 + \dfrac{0.4}{(1.6)^2}(x - 1.6)^2, & 0 < x < 1.6, \\ -0.5, & x \ge 1.6. \end{cases} \tag{5.5}$$

The wave speed $c(x)$ is given by

$$c(x) = \begin{cases} 0.6, & -0.4 < x < 0.4, \\ 1, & \text{otherwise.} \end{cases} \tag{5.6}$$

[2)] In fact, the fluctuation is not very small, since in practice the total time steps is a finite number. On average, we do observe that the error is decreased as refining the mesh.

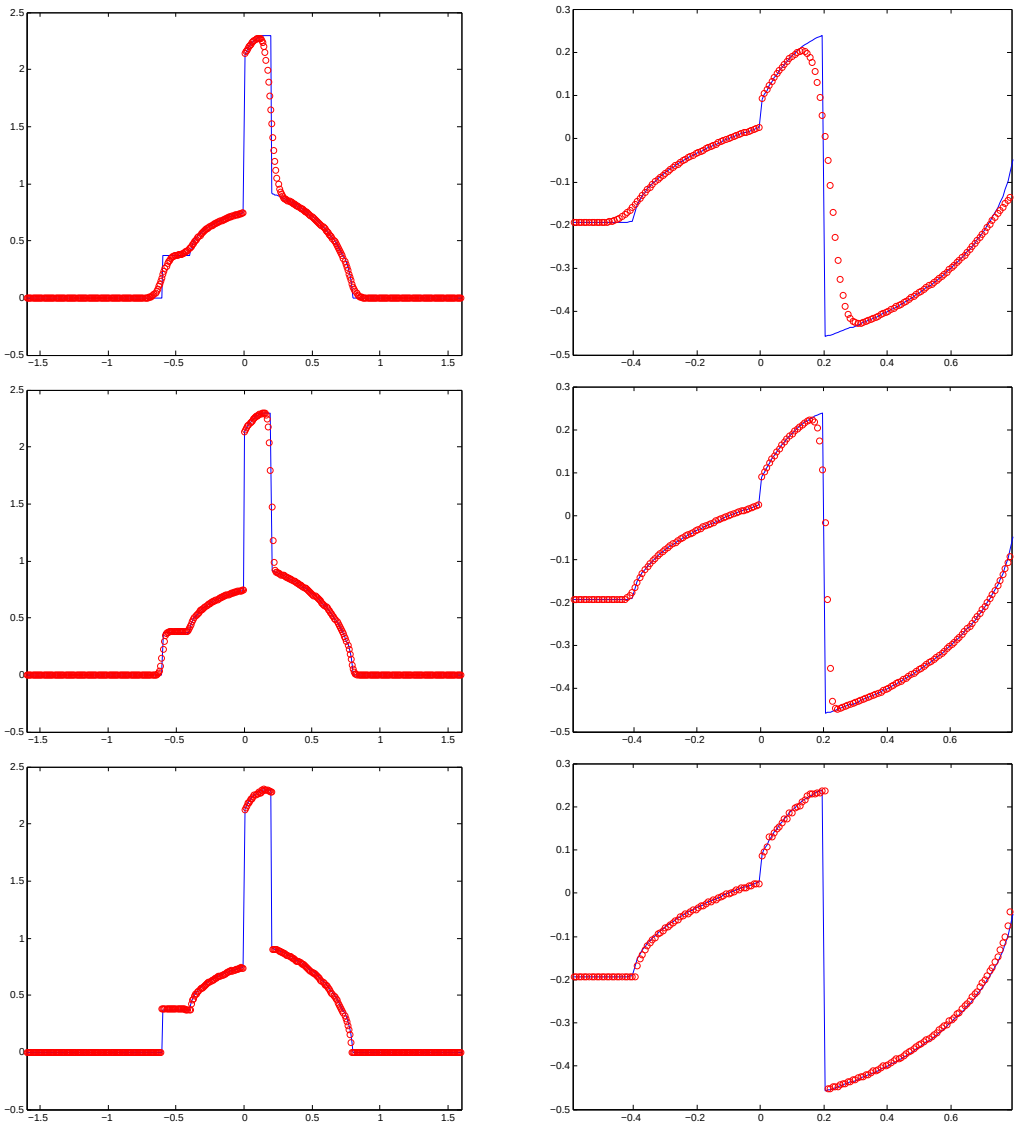

Fig. 5.2. Density ρ (left) and averaged slowness u (right) at $t = 1$. Solid line: exact solutions; $\circ$: numerical solutions. $h = 0.008$. CFL condition: $k = h$. Top: *upwind*; middle: *LW-lim*; bottom: QRCM.

The computational domain is $[x, v] \in [-1.6, 1.6] \times [-1.2, 1.2]$. Fig. 5.3 is an illustration of the initial and multi-valued slowness at $t = 1$. To solve the problem, we first discretize the initial delta function as [37]

$$\delta_w(x) = \begin{cases} \dfrac{1}{2w}\left(1 + \cos\left|\dfrac{\pi x}{w}\right|\right), & \left|\dfrac{x}{w}\right| \le 1, \\ 0, & \text{otherwise}, \end{cases} \tag{5.7}$$

where the parameter w is taken to be $w = 0.5\sqrt{\Delta x}$.

Fig. 5.4 shows the numerically computed ρ and u at time $t = 1$. The upwind solutions are smeared out badly during evolution. The *LW-lim* works better, but introduces oscillations

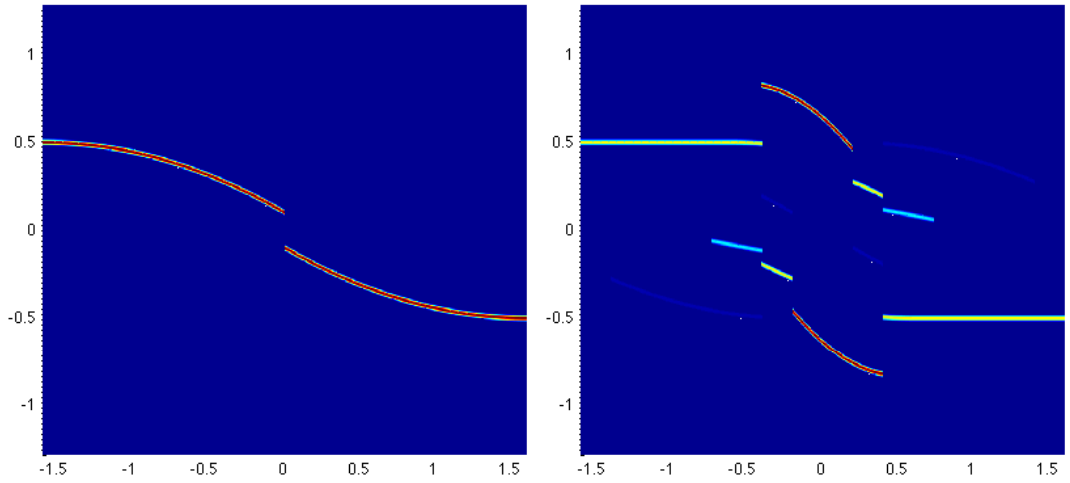

Fig. 5.3. Illustration of the initial slowness $u_0(x)$ and the multi-valued slowness at $t = 1$. The horizontal axis is x, the vertical axis is v.

around the discontinuities. This phenomenon is typical for a second-order method with limiter. A careful selection of the support size w in the approximate delta function can remove the oscillations, but the accuracy is lowered at the same time, see [14]. For the same reason, we skipped the *LW-lim* solutions in the next two 2-D examples. The l^1-errors of the solutions are reported in Table 5.2. For even measure-valued solutions, the QRCM still maintains the nearly first-order accuracy.

Table 5.2: l^1-errors of ρ at $t = 1$, $k = h/1.2$.

meshes	80×60	160×120	240×180	320×240	400×300	convergence rate
upwind	0.2282	0.1654	0.1364	0.1178	0.1054	**0.48**
LW-lim	0.1420	0.1026	0.0817	0.0703	0.0622	**0.51**
QRCM (avg)	0.0524	0.0213	0.0140	0.0102	0.0067	**1.23**

Example 4.3. We now consider the 2-D Liouville equation (4.1) with measure-valued solution. The wave speed is assumed to be

$$c(x,y) = \begin{cases} \sqrt{0.8}, & x > 0,\ y > 0, \\ \sqrt{0.6}, & \text{otherwise.} \end{cases} \tag{5.8}$$

The initial data is given by

$$f(x,y,u,v,0) = \delta(u-0.6)\delta(v-0.6). \tag{5.9}$$

For simplicity, we confine the problem to the region $[x,y,u,v] \in [-0.2,0.4]^2 \times [0.3,0.7]^2$. Then the exact density

$$\rho(x,y,t) = \iint f(x,y,u,v,t)\,dudv \tag{5.10}$$

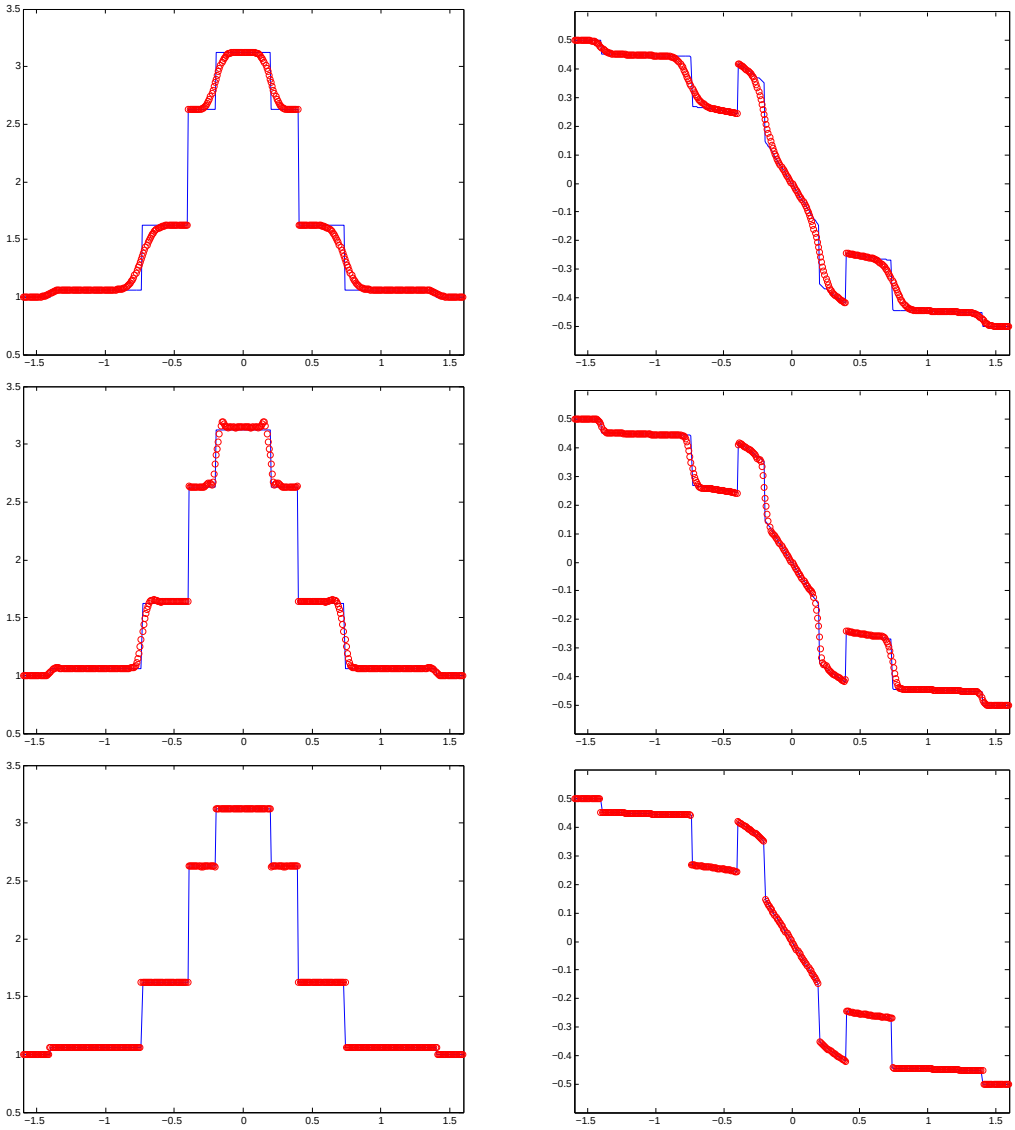

Fig. 5.4. Density ρ (left) and averaged slowness u (right) at $t = 1$. Solid line: exact solutions (see [14] for the analytical form); $\circ$: numerical solutions. $h = 0.008$. CFL condition: $k = h/1.2$. Top: *upwind*; middle: *LW-lim*; bottom: QRCM.

at $t = 0.4$ can be constructed as

$$\rho(x, y, 0.4) = \begin{cases} 1, & x < 0 \quad \text{or} \quad y < 0, \\ 1, & x > 0.4\sqrt{0.4}, \ y > 0.4\sqrt{0.4}, \\ \dfrac{3\sqrt{2}}{4}\alpha^T, & 0 < x < \dfrac{0.8\sqrt{0.6}}{3}, \ y > \sqrt{2}x, \\ \dfrac{3\sqrt{2}}{4}\alpha^T, & 0 < y < \dfrac{0.8\sqrt{0.6}}{3}, \ x > \sqrt{2}y, \\ 0, & \text{otherwise}, \end{cases} \tag{5.11}$$

where $\alpha^R = \left(\frac{\sqrt{2}-1}{\sqrt{2}+1}\right)^2$, $\alpha^T = 1 - \alpha^R$.

The numerical solutions are shown in Fig. 5.5. In 2-D, the situation is even worse: the upwind solution is far from the exact solution due to excessive numerical viscosity; the QRCM clearly provides a better result. The l^1-errors of solutions are given in Table 5.3. What we showed here for QRCM (and also in the next example) is the error of a single computation instead of average[3)] , i.e., for different meshes, we always pick the quasi-random numbers starting from the same index in the van der Corput sequence.

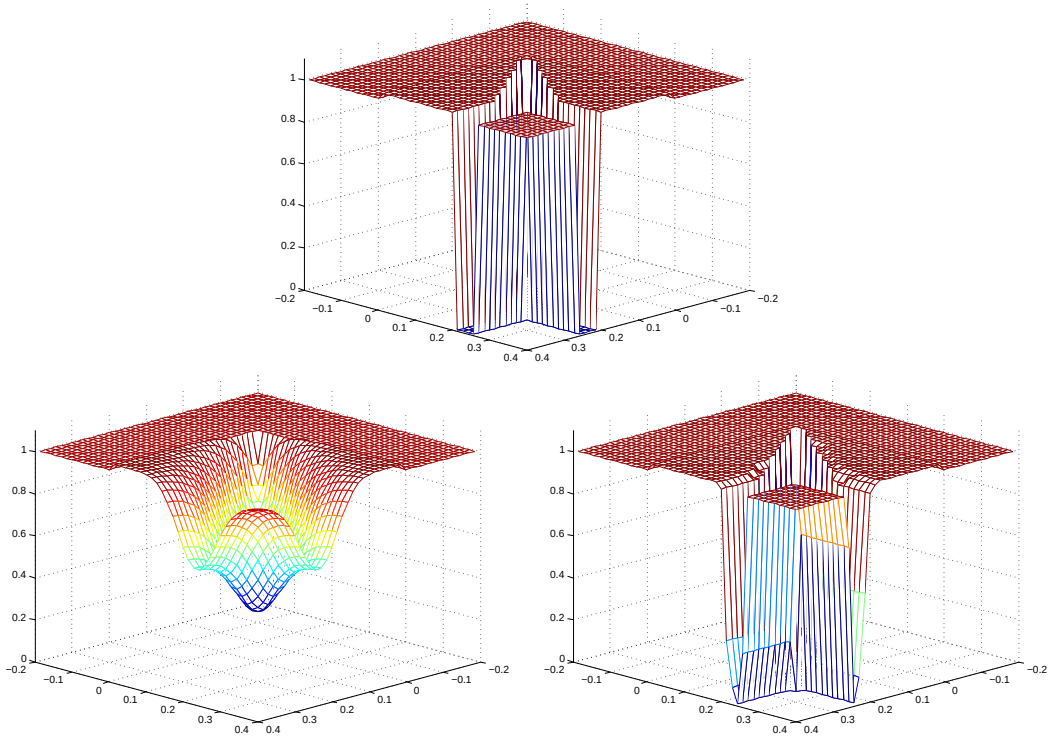

Fig. 5.5. The exact and numerical ρ at $t = 0.4$ on a 42×42 mesh. $h = 0.0143$. CFL condition: $k = h/2$. Top: exact solution; bottom left: *upwind*; bottom right: QRCM.

Table 5.3: l^1-errors of ρ at $t = 0.4$, $k = h/2$.

meshes	$18^2 \times 12^2$	$24^2 \times 16^2$	$30^2 \times 20^2$	$36^2 \times 24^2$	$42^2 \times 28^2$	convergence rate
upwind	0.0457	0.0416	0.0397	0.0374	0.0360	**0.28**
QRCM	0.0235	0.0141	0.0126	0.0103	0.0090	**1.08**

Example 4.4. We finally consider another 2-D example. Assume a beam of light travels from air to some medium, hitting the interface at an oblique angle. Then part of the light will be reflected back and part of it will be refracted into the medium in a different direction (see Fig. 5.6 for an illustration).

[3)] The error of QRCM for the 2-D equation seems to be more stable than 1-D. This may be because that more decisions are made for each quasi-random number — there are more possibilities than those in the 1-D case — which is equivalent to using longer quasi-random sequence in the simulation.

The problem can formulated mathematically as follows: let the wave speed be

$$c(x,y)=\begin{cases} c_l, & x<0,\\ c_r, & x>0, \end{cases} \tag{5.12}$$

with $c_l=1$, $c_r=2/3$. The initial condition is given by

$$f(x,y,u,v,0)=\rho_0(x,y)\delta(u-u_0)\delta(v-v_0), \tag{5.13}$$

where $u_0=1$, $v_0=1.6$, and

$$\rho_0(x,y)=\begin{cases} 1, & |y-v_0x/u_0-0.2|<0.05,\ -0.3<x<-0.1,\\ 0, & \text{otherwise.} \end{cases} \tag{5.14}$$

The exact density $\rho(x,y,t)$ at $t=0.4$ is given by

$$\begin{aligned} &\rho(x,y,0.4)\\ &=I_{\text{reg1}}\cdot\rho_0\left(x-\frac{0.4c_ru_0}{\sqrt{u_0^2+v_0^2}},\, y-\frac{0.4c_rv_0}{\sqrt{u_0^2+v_0^2}}\right)+I_{\text{reg2}}\cdot\rho_0\left(x-\frac{0.4u_0}{\sqrt{u_0^2+v_0^2}},\, y-\frac{0.4v_0}{\sqrt{u_0^2+v_0^2}}\right)\\ &\quad+I_{\text{reg3}}\cdot\alpha^R\rho_0\left(-x-\frac{0.4u_0}{\sqrt{u_0^2+v_0^2}},\, y-\frac{0.4v_0}{\sqrt{u_0^2+v_0^2}}\right)+I_{\text{reg4}}\cdot\alpha^T\frac{u_0}{c_r\sqrt{u_0^2+(1-c_r^2)v_0^2}}\\ &\quad\cdot\rho_0\left(\frac{u_0x}{c_r\sqrt{u_0^2+(1-c_r^2)v_0^2}}-\frac{0.4u_0}{\sqrt{u_0^2+v_0^2}},\, y-\frac{0.4v_0}{\sqrt{u_0^2+v_0^2}}+\frac{(1-c_r^2)v_0x}{c_r\sqrt{u_0^2+(1-c_r^2)v_0^2}}\right), \end{aligned} \tag{5.15}$$

where

$$\begin{aligned} I_{\text{reg1}}&=\left\{(x,y):\, x>\frac{0.4c_ru_0}{\sqrt{u_0^2+v_0^2}}\right\},\quad I_{\text{reg2}}=\{(x,y):\, x<0\},\\ I_{\text{reg3}}&=\left\{(x,y):\, -\frac{0.4u_0}{\sqrt{u_0^2+v_0^2}}<x<0\right\},\\ I_{\text{reg4}}&=\left\{(x,y):\, 0<x<\frac{0.4c_r\sqrt{u_0^2+(1-c_r^2)v_0^2}}{\sqrt{u_0^2+v_0^2}}\right\},\\ \alpha^R&=\left(\frac{c_ru_0-\sqrt{u_0^2+(1-c_r^2)v_0^2}}{c_ru_0+\sqrt{u_0^2+(1-c_r^2)v_0^2}}\right)^2,\quad \alpha^T=1-\alpha^R. \end{aligned} \tag{5.16}$$

Our computational domain is chosen as $x\in[-0.4,0.2]$, $y\in[-0.5,0.5]$, $u\in[-1.1,-0.9]\cup[0.9,1.1]\cup[2.25,2.45]$, $v\in[1.5,1.7]$ (the domain for u, v is chosen adaptively to minimize the computational cost). The numerical results and the l^1-errors are shown in Fig. 5.7 and Table 5.4 respectively. For this relatively large problem, one can barely see the shape of the exact solution for the upwind method, whereas the QRCM basically captures the correct shape and amplitude of the exact solution.

Table 5.4: l^1-errors of ρ at $t=0.4$, $k=h/2$.

h	0.04	0.02	0.01	0.005	convergence rate
upwind	0.0332	0.0275	0.0244	0.0198	**0.24**
QRCM	0.0171	0.0114	0.0044	0.0030	**0.89**

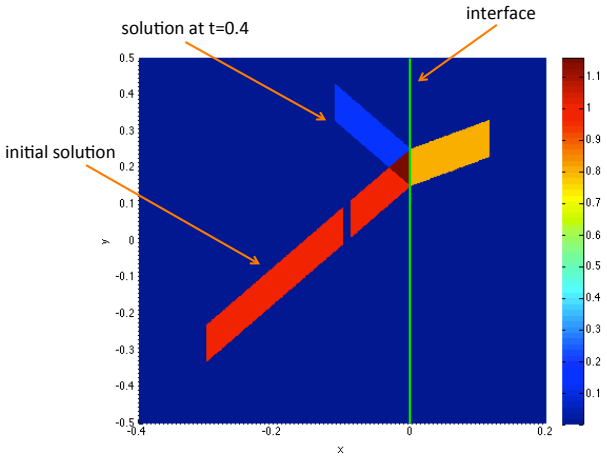

Fig. 5.6. Illustration of the geometry in the physical space. $x = 0$ is the interface. $x < 0$ is air. $x > 0$ is some medium with refractive index bigger than 1 (e.g., glass).

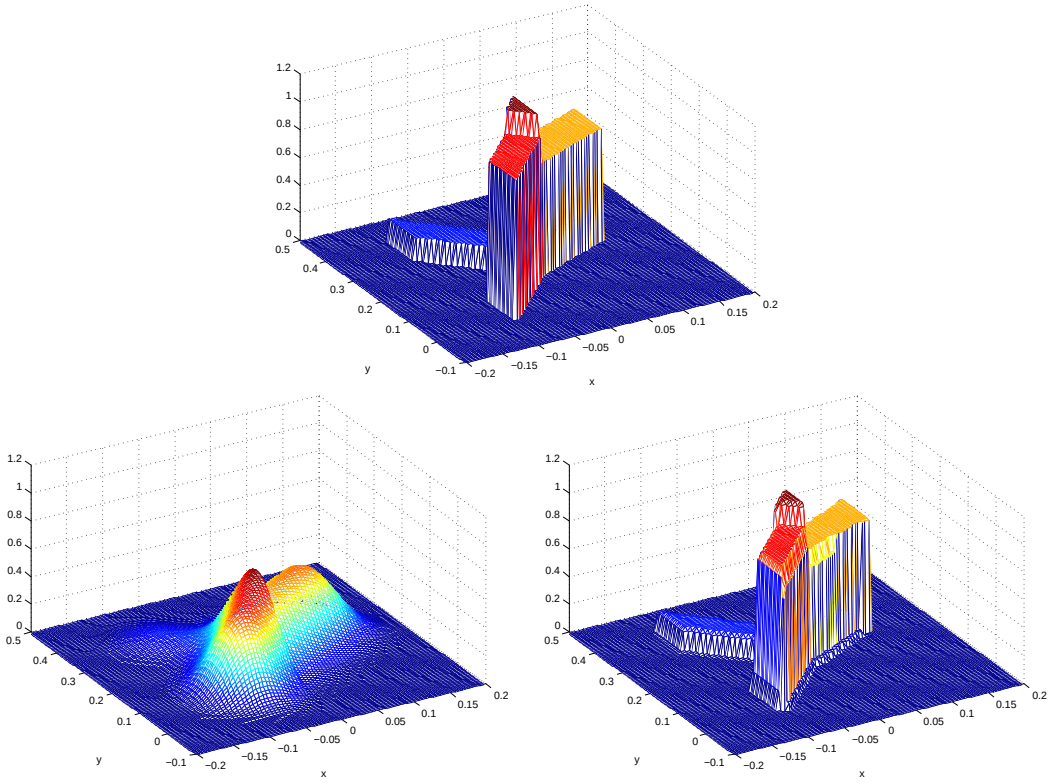

Fig. 5.7. The exact and numerical ρ at $t = 0.4$. $h = 0.005$. CFL condition: $k = h/2$. Top: exact solution; bottom left: *upwind*; bottom right: QRCM.

Acknowledgments. This work was partially supported by NSF grant DMS-0608720 and NSF FRG grant DMS-0757285. SJ was also supported by a Van Vleck Distinguished Research Prize and a Vilas Associate Award from University of Wisconsin-Madison.

Appendix A. The L^1-error estimate of the quasi-random choice method for the linear equation

In this appendix, we prove rigorously the L^1-error estimate of the QRCM for the linear equation:

$$u_t + au_x = 0, \quad x \in \mathbb{R},\ t > 0,\ a > 0, \tag{A.1}$$

$$u(x,0) = u_0(x), \quad x \in \mathbb{R}. \tag{A.2}$$

We assume that the initial data u_0 has bounded variation on $\mathbb{R}$, i.e.,

$$\|u_0\|_{BV(\mathbb{R})} = \sup \sum_{j=1}^{N} |u_0(x_j) - u_0(x_{j-1})| < \infty, \tag{A.3}$$

where the supremum is taken over all subdivisions of the real line $-\infty = x_0 < x_1 < \cdots < x_N = \infty$. Some techniques used here are similar to those in [38]. We have the following:

Theorem A.1. *Let $u(x,t)$ be the exact solution of (A.1) (A.2), and $\mathbf{U}^n(x,t)$ be the piecewise constant solution at t_n obtained by the QRCM, then*

$$\|u(\cdot,t_n) - \mathbf{U}^n(\cdot,t_n)\|_{L^1(\mathbb{R})} \le \left[C_1 \log\left(\frac{h}{k}t_n\right) h + C_2 \left|\log h\right| h\right] \|u_0\|_{BV(\mathbb{R})}. \tag{A.4}$$

Proof. Let $v(x,t)$ be the exact solution of (A.1) with initial data $\mathbf{U}^0(x,0)$ (the piecewise constant approximation of u_0), then

$$\|u(\cdot,t_n) - \mathbf{U}^n(\cdot,t_n)\|_{L^1(\mathbb{R})} \le \|u(\cdot,t_n) - v(\cdot,t_n)\|_{L^1(\mathbb{R})} + \|v(\cdot,t_n) - \mathbf{U}^n(\cdot,t_n)\|_{L^1(\mathbb{R})}. \tag{A.5}$$

Since equation (A.1) is linear, the first term on the right hand side of (A.5) can be bounded by

$$\|u(\cdot,t_n) - v(\cdot,t_n)\|_{L^1(\mathbb{R})} \le \|u_0(\cdot) - \mathbf{U}^0(\cdot,0)\|_{L^1(\mathbb{R})} \le h\|u_0\|_{BV(\mathbb{R})}. \tag{A.6}$$

To estimate the second term $\|v(\cdot,t_n) - \mathbf{U}^n(\cdot,t_n)\|_{L^1(\mathbb{R})}$, we decompose the initial data $\mathbf{U}^0(x,0)$ in the following way:

$$\mathbf{U}^0(x,0) = \sum_{i=-\infty}^{\infty} w_i(x), \tag{A.7}$$

where

$$w_i(x) = \begin{cases} 0, & x < \left(i + \dfrac{1}{2}\right) h, \\ U^0_{i+1} - U^0_i, & x > \left(i + \dfrac{1}{2}\right) h. \end{cases} \tag{A.8}$$

Let $v_{w_i}(x,t)$, $\mathbf{U}^n_{w_i}(x,t)$ denote respectively the exact and the QRCM solutions with initial data $w_i(x)$, then

$$\begin{aligned} \|v(\cdot,t_n) - \mathbf{U}^n(\cdot,t_n)\|_{L^1(\mathbb{R})} &= \left\| \sum_{i=-\infty}^{\infty} \left[v_{w_i}(\cdot,t_n) - \mathbf{U}^n_{w_i}(\cdot,t_n)\right] \right\|_{L^1(\mathbb{R})} \\ &\le \sum_{i=-\infty}^{\infty} \|v_{w_i}(\cdot,t_n) - \mathbf{U}^n_{w_i}(\cdot,t_n)\|_{L^1(\mathbb{R})}. \end{aligned} \tag{A.9}$$

Assume the same quasi-random sequence is used for all w_i. From the discussion in Section 3, we know

$$\|v_{w_i}(\cdot,t_n)-\mathbf{U}^n_{w_i}(\cdot,t_n)\|_{L^1(\mathbb{R})}\le\frac{h}{k}t_n\left|\delta(\boldsymbol{\xi},n,I)\right|\left|U^0_{i+1}-U^0_i\right|, \tag{A.10}$$

where $I=[0,ak/h)$. Therefore,

$$\begin{aligned}\|v(\cdot,t_n)-\mathbf{U}^n(\cdot,t_n)\|_{L^1(\mathbb{R})}&\le\frac{h}{k}t_n\left|\delta(\boldsymbol{\xi},n,I)\right|\sum_{i=-\infty}^{\infty}\left|U^0_{i+1}-U^0_i\right|\\&\le\frac{h}{k}t_n\left|\delta(\boldsymbol{\xi},n,I)\right|\|u_0\|_{BV(\mathbb{R})}\\&\le C\frac{h}{k}t_n\frac{\log n}{n}\|u_0\|_{BV(\mathbb{R})}.\end{aligned} \tag{A.11}$$

To sum up

$$\begin{aligned}\|u(\cdot,t_n)-\mathbf{U}^n(\cdot,t_n)\|_{L^1(\mathbb{R})}&\le h\|u_0\|_{BV(\mathbb{R})}+C\frac{h}{k}t_n\frac{\log n}{n}\|u_0\|_{BV(\mathbb{R})}\\&\le\left[h+C\log\left(\frac{h}{k}\frac{t_n}{h}\right)h\right]\|u_0\|_{BV(\mathbb{R})}\\&\le\left[C_1\log\left(\frac{h}{k}t_n\right)h+C_2\left|\log h\right|h\right]\|u_0\|_{BV(\mathbb{R})}.\end{aligned} \tag{A.12}$$

References

[1] P.L. Lions and T. Paul, Sur les mesures de Wigner, *Rev. Math. Iberoamericana*, **9** (1993), 553–618.

[2] L. Ryzhik, G. Papanicolaou and J.B. Keller, Transport equations for elastic and other waves in random media, *Wave Motion*, **24** (1996), 327–370.

[3] P. Gérard, P.A. Markowich, N.J. Mauser and F. Poupaud, Homogenization limits and Wigner transforms, *Commun. Pure Appl. Math.*, **50** (1997), 323–379.

[4] B. Engquist, O. Runborg and A.K. Tornberg, High-frequency wave propagation by the segment projection method, *J. Comput. Phys.*, **178** (2002), 373–390.

[5] S. Fomel and J.A. Sethian, Fast-phase space computation of multiple arrivals, *Proc. Nat. Acad. Sci. U.S.A.*, **99** (2002), 7329–7334.

[6] S. Jin and S. Osher, A level set method for the computation of multivalued solutions to quasi-linear hyperbolic PDEs and Hamilton-Jacobi equations, *Comm. Math. Sci.*, **1** (2003), 575–591.

[7] B. Engquist and O. Runborg, Computational high frequency wave propagation, *Acta Numerica*, **12** (2003), 181–266.

[8] L.T. Cheng, M. Kang, S. Osher, H. Shim and Y.H. Tsai, Reflection in a level set framework for geometric optics, *Comput. Model. Eng. Sci.*, **5** (2004), 347–360.

[9] F. Nier, Asymptotic analysis of a scaled Wigner equation and quantum scattering, *Transp. Theory Stat. Phys.*, **24** (1995), 591–629.

[10] F. Nier, A semi-classical picture of quantum scattering, *Ann. Sci. Ec. Norm. Sup.*, **29** (1996), 149–183.

[11] G. Bal, J.B. Keller, G. Papanicolaou and L. Ryzhik, Transport theory for acoustic waves with reflection and transmission at interfaces, *Wave Motion*, **30** (1999), 303–327.

[12] L. Miller, Refraction of high frequency waves density by sharp interfaces and semiclassical measures at the boundary, *J. Math. Pures Appl.*, **79** (2000), 227–269.

[13] S. Jin and X. Wen, Hamiltonian-preserving schemes for the Liouville equation of geometrical optics with discontinuous local wave speeds, *J. Comput. Phys.*, **214** (2006), 672–697.

[14] S. Jin and X. Wen, A Hamiltonian-preserving scheme for the Liouville equation of geometrical optics with partial transmissions and reflections, *SIAM J. Numer. Anal.*, **44** (2006), 1801–1828.
[15] S. Jin and K.A. Novak, A semiclassical transport model for thin quantum barriers, *Multiscale Model. Simul.*, **5** (2006), 1063–1086.
[16] S. Jin, H. Wu and Z. Huang, A hybrid phase-flow method for Hamiltonian systems with discontinuous Hamiltonians, *SIAM J. Sci. Comput.*, **31** (2008), 1303–1321.
[17] S. Jin and K.A. Novak, A coherent semiclassical transport model for pure-state quantum scattering, *Comm. Math. Sci.*, **8** (2010), 253–275.
[18] D. Wei, S. Jin, R. Tsai and X. Yang, A level set method for the semiclassical limit of the Schrödinger equation with discontinuous potentials, *J. Comput. Phys.*, **229** (2010), 7440–7455.
[19] A. Harten, The artificial compression method for computation of shocks and contact discontinuities. I. Single conservation laws, *Commun. Pure Appl. Math.*, **30** (1977), 611–638.
[20] S. Jin, H. Liu, S. Osher and R. Tsai, Computing multi-valued physical observables for the high frequency limit of symmetric hyperbolic systems, *J. Comput. Phys.*, **210** (2005), 497–518.
[21] J. Glimm, Solutions in the large for nonlinear hyperbolic systems of equations, *Commun. Pure Appl. Math.*, **18** (1965), 697–715.
[22] A.J. Chorin, Random choice solution of hyperbolic systems, *J. Comput. Phys.*, **22** (1976), 517–533.
[23] A.J. Chorin, Random choice methods with applications to reacting gas flow, *J. Comput. Phys.*, **25** (1977), 253–272.
[24] G.A. Sod, A numerical study of a coverging cylindrical shock, *J. Fluid Mech.*, **83** (1977), 785–794.
[25] P. Concus and W. Proskurowski, Numerical solution of a nonlinear hyperbolic equation by the random choice method, *J. Comput. Phys.*, **30** (1979), 153–166.
[26] P. Colella, Glimm's method for gas dynamics, *SIAM J. Sci. Stat. Comput.*, **3** (1982), 76–110.
[27] C.Y. Loh, M.S. Liou and W.H. Hui, An investigation of random choice method for three-dimensional steady supersonic flows, *Int. J. Numer. Methods Fluids*, **29** (1999), 97–119.
[28] A. Jazcilevich and V. Fuentes-Gea, The conservative random choice method for the numerical solution of the advection equation, *Monthly Weather Review*, **127** (1999), 2281–2292.
[29] X. Wen, A high order numerical method for computing physical observables in the semiclassical limit of the one dimensional linear Schrödinger equation with discontinuous potentials, *J. Sci. Comput.*, **42** (2010), 318–344.
[30] B.J. Lucier, Error bounds for the methods of Glimm, Godunov and LeVeque, *SIAM J. Numer. Anal.*, **22** (1985), 1074–1081.
[31] H. Niederreiter, Random Number Generation and Quasi-Monte Carlo Methods, SIAM, Philadelphia, PA, 1992.
[32] J.G.van der Corput, Verteilungsfunktionen, *Proc. Ned. Akad. v. Wet.*, **38** (1935), 813–821.
[33] R.E. Caflisch, Monte Carlo and quasi-Monte Carlo methods, *Acta Numerica*, (1998), 1–49.
[34] R.J. LeVeque, Numerical Methods for Conservation Laws, Birkhäuser Verlag, Basel, second edition, 1992.
[35] N.N. Kuznetsov, Accuracy of some approximate methods for computing the weak solutions of a first-order quasi-linear equation, *USSR Comput. Math. Math. Phys.*, **16** (1976), 105–119.
[36] T. Tang and Z.H. Teng, The sharpness of Kuznetsov's $O(\sqrt{\Delta x})$ L^1-error estimate for monotone difference schemes, *Math. Comput.*, **64** (1995), 581–589.
[37] B. Engquist, A.K. Tornberg and R. Tsai, Discretization of Dirac delta functions in level set methods, *J. Comput. Phys.*, **207** (2005), 28–51.
[38] S. Jin and X. Wen, Convergence of an immersed interface upwind scheme for linear advection equations with piecewise constant coefficients I: L^1-error estimates, *J. Comput. Math.*, **26** (2008), 1–22.